ORIGINAL ARTICLE

A model and its experiment using compressed cold air to clean the active surface of a grinding wheel during sharping of a hob cutter

Wojciech Stachurski[1] · Jacek Sawicki[3] · Krzysztof Krupanek[3] · Krzysztof Nadolny[2]

Abstract

The removal of chips, which is produced during the grinding process and forms, among other things, cloggings on the grinding wheel active surface (GWAS), is key to extending wheel life and achieving low surface roughness. Currently, as a result of the minimum quantity lubrication (MQL) method of delivery coolant into the cutting zone, the support of chips removal with a stream of cooled compressed air (CCA) is becoming particularly important. Among other things, the angle of the CCA jet delivery nozzle with respect to the GWAS is responsible for the removal efficiency, which has to be considered individually for each grinding process variation, and experimental tests alone do not give an idea of the CCA jet flow. In the present study, a numerical flow analysis (using the computational fluid dynamics method) of cooled compressed air in the grinding zone during the sharpening of a hob cutter face was carried out. The results of the numerical simulations were verified experimentally by determining the percentage of the grinding wheel clogging $Z_\%$. The experimental results confirmed the conclusions from the numerical analysis regarding the most favorable angle of the CCA nozzle. The $Z_\% = 5.3$ clogging index obtained when grinding with the CCA nozzle set at an angle of 45° is 2.5 times lower than the $Z_\% = 13.5$ index determined for the most favorable setting of the MQL nozzle. Simultaneous delivery of CCA and air-oil aerosol using the MQL-CCA method resulted in the lowest $Z_\% = 2.5$, comparable to the $Z_\% = 2.0$ obtained for a grinding wheel operating under cooling conditions with a water-based oil emulsion delivered by the flood method (WET).

Keywords Hob cutters · Grinding process · Compressed cold air · Numerical simulation · Grinding wheel clogging

Abbreviations

CAG	Cold air gun
CCA	Compressed cold air
CFD	Computational fluid dynamics
CMOS	Complementary metal–oxide–semiconductor
GWAS	Grinding wheel active surface
HRC	Hardness in Rockwell C scale
LED	Light-emitting diode
MQL	Minimum quantity lubrication
MQL-CCA	Combined MQL and compressed cold air (CCA)
RANS	Reynolds-averaged Navier–Stokes equations
SST	Shear stress transport turbulence model
WET	Flood method using water emulsion as coolant
a	Machining allowance (mm)
a_e	Working engagement (mm)
d	Nozzle outlet diameter (mm)
m	Module (mm)
$\dot{m}_{in}$	Mass flow of air on inlet surface into the fluid domain (kg/s)
$\dot{m}_{out}$	Mass flow of air on outlet surface into the fluid domain (kg/s)
n_s	Grinding wheel rotational speed (rpm)

✉ Krzysztof Nadolny
krzysztof.nadolny@tu.koszalin.pl

Wojciech Stachurski
wojciech.stachurski@p.lodz.pl

Jacek Sawicki
jacek.sawicki@p.lodz.pl

Krzysztof Krupanek
krzysztof.krupanek@dokt.p.lodz.pl

[1] Institute of Machine Tools and Production Engineering, Lodz University of Technology, Stefanowskiego 1/15, 90-537 Lodz, Poland

[2] Department of Production Engineering, Faculty of Mechanical Engineering, Koszalin University of Technology, Racławicka 15-17, 75-620, Koszalin, Poland

[3] Institute of Materials Science and Engineering, Lodz University of Technology, Stefanowskiego 1/15, 90-537 Lodz, Poland

p_{CCA}	Air pressure for CCA jet grinding (MPa)
P_τ	Area of wall shear stress (mm^2)
Q_d	Diamond dresser mass (kt)
Q_{MQL}	MQL fluid flow rate (ml/h)
Q_{WET}	Coolant flow rate in flood method (l/min)
T_{CCA}	CCA temperature (°C)
v_s	Grinding wheel peripheral speed (m/s)
v_w	Workpiece peripheral speed (m/min)
z_h	Number of cutting blades (hob cutter)
$Z_\%$	Percentage rate of grinding wheel clogging (%)
α	Pressure angle (°)
ε	Angle of nozzle inclination during coolant delivery (°)
η_{ws}	Efficiency of system delivering air directly into the grinding zone
τ_w	Wall shear stress (Pa)
$\tau_w\text{-}_{max}$	Maximum wall shear stress (Pa)

1 Introduction

The current pursuit to achieve sustainable manufacturing is one of the most important challenges in the manufacturing industry [1–3]. The possibility of sustainable manufacturing using abrasive machining processes depends mainly on neutralizing the risks posed by the use of cooling and lubricating fluids (coolants) [4, 5]. Currently, they are still commonly used in the form of oils or aqueous oil emulsions and are most often supplied to the machining zone in high volume mode using the flooding (WET) method with high flow rates, up to 15 l/min (900,000 ml/h) [6, 7]. Despite their known advantages [8], they are nevertheless considered undesirable due to the risk to the environment [9], the health of machine tool operators [10], and the high cost of use [11, 12].

In view of the above, research work on ensuring sustainable manufacturing in various areas of the abrasive machining process is being carried out in global research centers. An example is a novel approach to machining presented in [13], whose authors described a new chemical–mechanical polishing slurry and its polishing mechanisms on a nickel alloy developed for production in the semiconductor, microelectronics, and aerospace industries. Another example in this area is research on the development of a type of new chemical–mechanical polishing slurry for copper including environmentally friendly compositions [14]. Based on the work in [15, 16], it should be stated that theories and models are important for grinding and abrasive machining to understand machining processes and play an important role in the development of new approaches to machining. Their authors have developed a novel model for maximum undeformed chip thickness that is in good agreement with those in grinding experiments. Another example of a novel approach is the work in [17–19]. A novel approach to single-grain scratching at 40.2 m/s and nanoscale depth of cut has been carried out, in which the speeds used are four to seven orders of magnitude higher than those used in nanogrinding. Thanks to groundbreaking theories, new methods of mechanical chemical grinding have been developed [20, 21] and high-performance surfaces that are extremely difficult to produce by traditional means have been produced.

Among other ways of neutralizing the deleterious effects of coolants, the method of minimized coolant output, denoted by the acronym MQL (minimum quantity lubrication), has gained great popularity [22–24]. In this method, an air-oil aerosol stream is delivered with a coolant output of only 10–500 ml/h [25–31]. The literature shows [32, 33] that under specific processing conditions, the use of the MQL method gives results comparable to the flood method [34–39].

Studies by the authors [40] of this article related to the application of the MQL method in the grinding process of hob cutter contact surfaces, however, pointed out the insufficient cleaning capacity of the MQL method, understood as the limited ability to remove machining products from the grinding zone. A solution to this problem can be the use of an additional cleaning nozzle using a stream of compressed air [41–43] or cooled compressed air. A vortex tube refrigeration method using cold air guns (CAG) nozzles [44] is used to cool the compressed air stream. The available literature indicates that the simultaneous application of the MQL and CCA methods creates the possibility of effective cooling and lubrication in the machining zone [45–48]. This is also confirmed by the authors' experimental studies [49, 50] describing the grinding of the hob cutter [51]. This method, designated by the acronym MQL-CCA, made it possible to achieve a technological state of the surface layer at the level of values obtained after machining with coolants supplied by the flood method (WET). However, the literature indicates the possibility of further improvement of grinding results, specifying that the effectiveness of the effect of any coolants significantly depends on the angular position of the nozzle relative to the active surface of the grinding wheel (GWAS), and this should be considered individually for each variation of the grinding process [52–55]. Unfortunately, in this context, experimental studies alone do not make it possible to perform the necessary analysis of the CCA flow in the grinding zone during the grinding of the hob cutter face. For this reason, it is necessary to perform numerical simulations of such flow for different nozzle settings, while due to the different geometry and kinematics of this variety of grinding, it is not possible to use the results of studies available in the literature [56–62]. These will allow a precise analysis of the phenomena accompanying the flows and the identification of the most favorable angular setting of the grinding wheel from the viewpoint of GWAS cleaning.

In view of the above, the purpose of the research described in this article is to evaluate the ability of CCA to

clean GWAS during the sharpening of hob cutters. The evaluation is based on numerical simulations of CCA flow and verification experimental studies. "Section 2" describes the steps related to the preparation of the geometric model and mesh, the establishment of boundary and initial conditions, and the simulation of the flow based on the "SST k-ω" model available in Ansys CFX software using the Kato-Launder modification. Based on the results obtained ("Sect. 3"), a parameter was determined that describes the ratio of the amount of air delivered by the nozzle to the grinding zone to the amount of air entering directly into the zone of contact between the grinding wheel and the hob cutter – the efficiency η_{ws} of the air delivery system. The value of the tangential shear stress τ_w occurring on the conical surface of the grinding wheel in the area of the wheel's active surface and the area of the surface P_τ affected by these stresses were also determined. "Section 4" describes experimental studies that verify the results of numerical simulations. The amount of cloggings occurring on the GWAS, defined as the percentage rate $Z_\%$ of the wheel's clogging, was used as a parameter for verifying the cleaning efficiency of the grinding wheel. This index was determined by analyzing microscopic images of the GWAS. The methodology, in a similar form, was also used by other researchers [63, 64].

The research work in the area described in this article is new and has not been undertaken before, and the results have application potential for both scientific and industrial aspects.

2 Numerical simulation of the flow of compressed cold air in the grinding zone during the sharpening of hob cutters' face

2.1 Machining conditions and 3D CAD models

Before carrying out the numerical simulations, 3D CAD models of the actual components involved in the grinding process of the hob cutter face were made. Figure 1 shows the machining space of a specialized tool grinding machine for sharpening hob cutters. During grinding, the hob cutter 1 is mounted on a tool arbor 2 and moves with the grinding table at a speed v_w relative to the grinding wheel 3 rotating at a speed n_s. The machining allowance a is removed as a result of the mutual movement of the grinding wheel and the hob cutter in successive cycles. Within each cycle, which consists of a grinding and return stroke (Fig. 1), the allowance a_e is removed. The coolant is delivered to the grinding zone through a single nozzle. In the case under consideration, this constitutes nozzle 4, spraying compressed cold air (CCA).

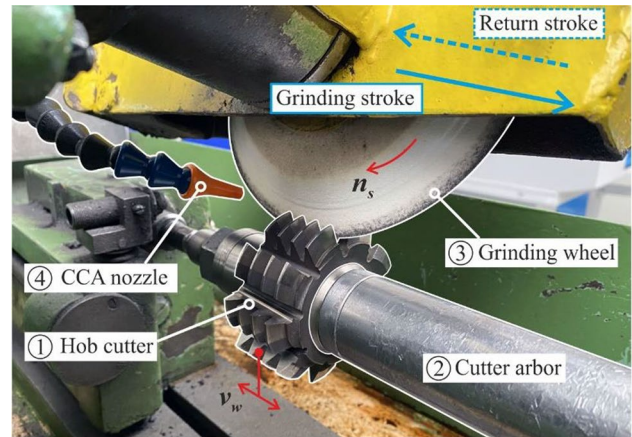Three 3D CAD models were made for the numerical simulations, namely models for (1) the hob cutter, (2) the

Fig. 1 View of the machining zone during grinding the face of a hob cutter

grinding wheel, and (3) the CAG (Cold Air Guns) nozzle used to feed compressed cold air (CCA) into the grinding zone. In the case of the CAG nozzle model, it was decided to create only a model of the nozzle tip itself for the purpose of the research being conducted. It was assumed that this model, hereinafter referred to as the CCA nozzle, would be a solid with a circular cross-section and a diameter of $d = 5$ mm, corresponding to the nozzle outlet diameter used in the experimental tests. The complete set of assumptions made to create the 3D CAD models is summarized in Table 1.

It should be noted that the value of module m of the hob cutter was selected as the upper value from the range of modules of hob cutters most commonly used in the automotive industry in the production of passenger car parts. In practice, this makes it possible to obtain the most technologically difficult working conditions resulting from the longest maximum contact distance between the abrasive grains of the grinding wheel active surface and the machined surface.

According to the manufacturer's data [66], the WNT 6910.15.3–7 nozzle can operate at a supply pressure in the range of 0.3–0.7 MPa, allowing it to produce a compressed air stream with a temperature even up to 55 ℃ lower than the temperature value of the air supplying the nozzle. For the purpose of the research, experimental measurements of the T_{CCA} temperature of compressed cold air obtained at the outlet of the CAG nozzle were made, depending on the value of the supply pressure p_{CCA}. An M890G digital multimeter equipped with a K-type thermocouple measuring probe was used to measure the temperature. The reading resolution of the multimeter is 1 ℃. The lowest temperature (-20 ℃) was obtained at the nozzle outlet when the supply pressure $p_{CCA} = 0.6$ MPa was set. Due to the fact that the CAG nozzle outlet is located at a distance of about 10 mm from the grinding wheel active surface, the temperature of the

Table 1 Parameters of 3D CAD models

CAD 3D model	
Element	Parameters
Hob cutter	- Solid hob cutter for hobbing gears according to ISO 53 and ISO 54 - Module $m = 3$ mm, - Pressure angle $\alpha = 20°$ - Number of cutting edges $z_h = 9$ - Normal ground profile - Geometric dimensions were selected according to PN-ISO 4468:1999 - Accuracy class B (acc. to PN-ISO 4468:1999)
Grinding wheel	- Disc wheel type 12 acc. to PN-ISO 525:2001 - Dimensions: $200/90 \times 20/2 \times 32$ acc. to Norton catalogue [65]
CCA nozzle	- A single CAG nozzle, symbol WNT 6910.15.3–7 [66] - Nozzle outlet diameter $d = 5$ mm

compressed cold air was measured at various distances from the nozzle outlet. The measurement results are presented in Table 2, and the value $T_{CCA} = -20$ °C obtained at the distance $l = 15$ mm was used in the further part of the research.

2.2 3D CAD model of the system and supply of compressed cold air by CCA

Before performing the numerical simulations, the created 3D CAD models were mutually arranged in a way that corresponds to the actual positions of the mapped components during the sharpening process. A 3D CAD model of the system was thus created (Figs. 2 and 3).

As shown in Fig. 2, a stream of compressed cold air is delivered to the grinding zone by means of a nozzle, on the left side of the hob cutter 2, on the CCA fragment of the active surface of the grinding wheel 1. The CCA area is located between line X, which is the line of contact between the apical cutting edges of the hob cutter and the grinding wheel, and the conventional line Y located parallel to line X at a distance of 25 mm from it. Such a location of the CCA area results from the information contained in sources in the literature, a review of which showed that a stream of compressed cold air should be applied to the grinding wheel active surface (GWAS) as close as possible to the contact zone between the grinding wheel and the workpiece [53]. Locating this area, as shown in Fig. 2,

eliminates the occurrence of collisions resulting from the respective movement of the grinding wheel and the cutter during machining.

As shown in Fig. 3, the axis of nozzle 3 is inclined at an angle of 90° to line C, defined by the form of the cone describing the grinding wheel body (Fig. 3b), and then at an angle ε to line D (Fig. 3c), which is tangential to the active surface of the grinding wheel and simultaneously intersects line C at an angle of 90° (Fig. 3a). As shown in Fig. 3c, four settings of the angle ε were used in the tests, which were respectively: 30°, 45°, 60°, and 90°. At the same time, it should be mentioned that the angular inclination of nozzle 3 with respect to line D must not be less than 30°, due to technical limitations in nozzle positioning. Moreover, the outlet of nozzle 3 was placed at a distance of 15 mm from the grinding wheel active surface. The grinding wheel, rotating clockwise, after withdrawing
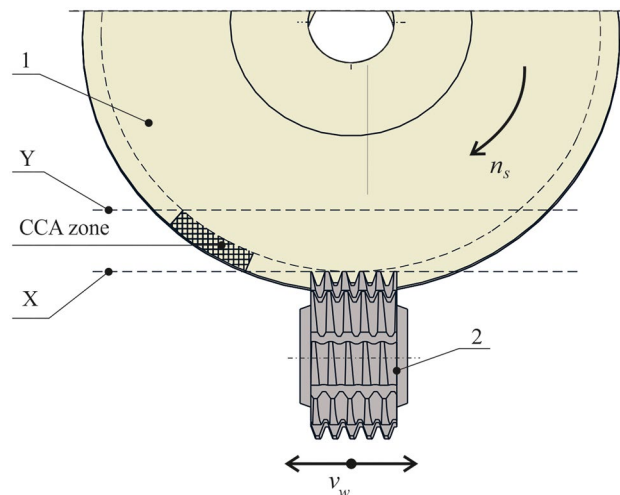
Table 2 T_{CCA} temperature of compressed cold air stream (CCA)

Supply pressure p_{CCA} [MPa]	Distance from nozzle outlet l [mm]						
	0	5	10	13	15	17	20
	Temperature T [°C]						
0.6	−20	−20	−20	−20	−20	−17	−15

Fig. 2 Location of area on grinding wheel active surface on which flow of cooled compressed cold air was directed (CCA area); 1 – grinding wheel, 2 – hob cutter, X – contact line of the hob cutter cutting edges with the grinding wheel, Y – conventional line parallel to X

Fig. 3 Angular arrangement of the compressed cold air supply (CCA) nozzle relative to the grinding wheel active surface: **a** general view, **b** positioning of the CCA nozzle relative to line C, **c** positioning of the CCA nozzle relative to line D; 1 – grinding wheel, 2 – hob cutter, 3 – CCA nozzle, C – line drawn through the cone formation of the grinding wheel, D – line tangential to the grinding wheel active surface
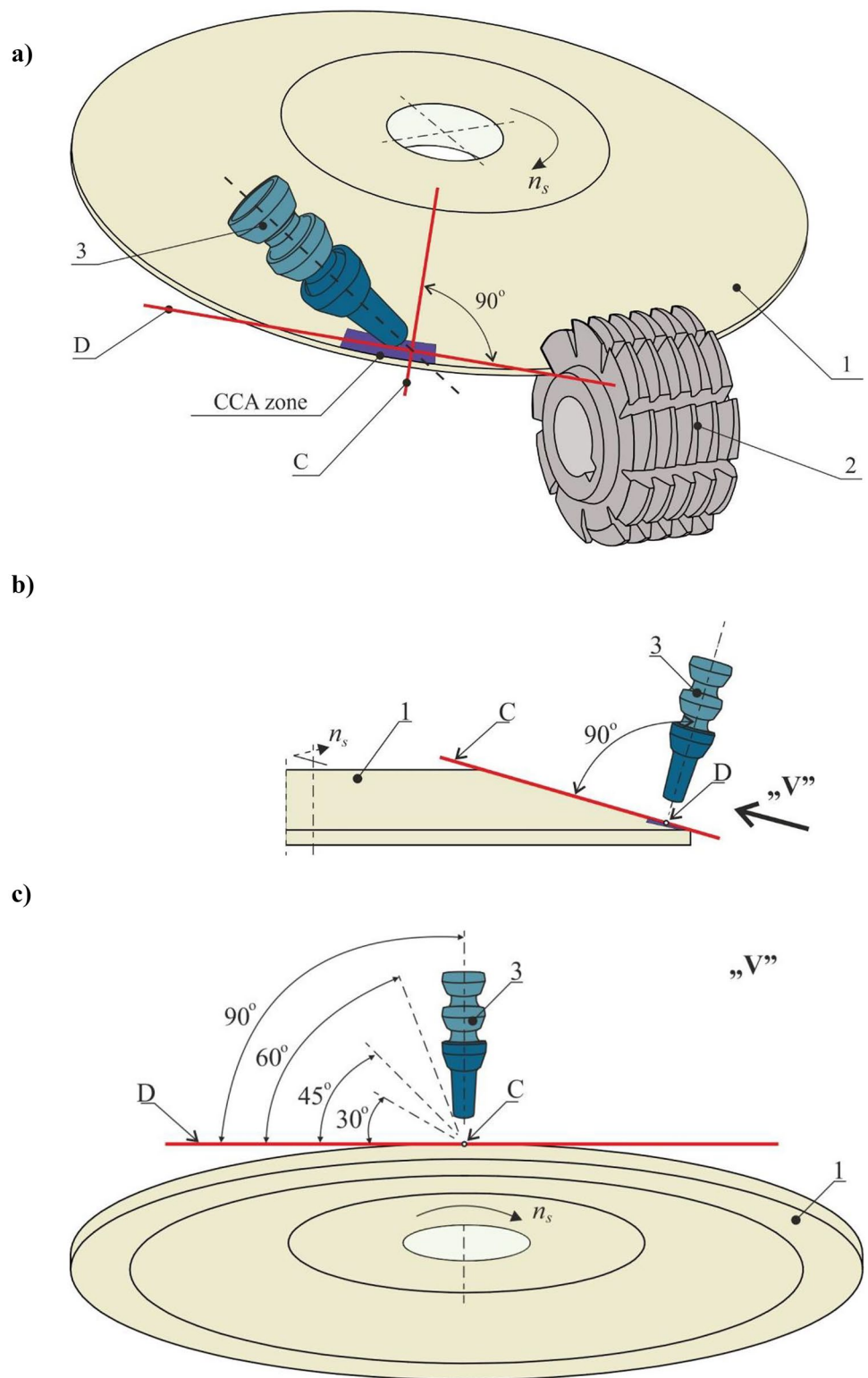
from contact with the workpiece surface, is cleaned by the compressed cold air jet (CCA). In the case of simultaneous application of the MQL method and administration of compressed cold air (CCA), as it is the case with the MQL-CCA method, the wheel rotates and lifts the oil mist supplied by the MQL nozzle into the grinding zone and is then cleaned of the grinding products by the compressed cold air jet supplied by the CAG nozzle.
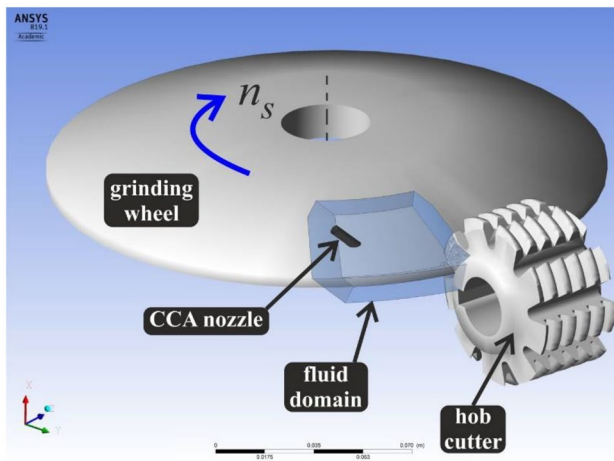
Fig. 4 Location of fluid domain within 3D model of CCA air supply system

2.3 Numerical simulation of air flow in CCA method

2.3.1 Simulation model and computational grid

The aim of the conducted simulation studies was to determine the capacity of the air supplied by the CAG nozzle during the sharpening of hob cutters for GWAS cleaning. The most important specific objectives of the numerical simulations carried out were as follows.

1. Determination of the parameter defining the ratio of the amount of air delivered by the CAG nozzle to the grinding zone to the amount of air entering directly into the contact zone of the grinding wheel with the hob cutter. It was assumed that this parameter would be defined as the efficiency η_{ws} of the air supply system when using a CCA jet.

2. Determination of the value of wall shear stress τ_w occurring on the conical surface of the grinding wheel in the area of active surface of the wheel as a result of air supply using the CCA method.

3. Determination of surface area P_τ affected by wall shear stress τ_w.

In the course of the research, a flow of compressed cold air was simulated, which after being discharged from a nozzle reaches the grinding wheel active surface rotating with the rotational speed n_s. The area in which the air flow was simulated was defined by the fluid domain, located between the elements of the 3D model of the system and matching the shape of the grinding wheel, hob cutter, and nozzle tip (Fig. 4).

Prior to simulation, the fluid domain was optimized by creating hexagonal grid elements whose regular shapes allow for correct results in numerical simulation. Particular emphasis was placed on the consistency of the grid and the appropriate thickening of the inflation layer at the point of contact between the air and the surface of the rotating grinding wheel. The appearance of the fluid domain grids optimized for the simulation is shown in Fig. 5. Depending on the nozzle angle, the number of nodes in the model ranged from 2,119,321 to 5,128,077, while the number of elements ranged from 2,110,772 to 5,449,291. Detailed values of the number of nodes and elements for each discrete model are presented in Table 3 at the end of this chapter.

2.3.2 Boundary and initial conditions

Numerical simulations to determine the efficiency η_{ws}, the wall shear stress τ_w, and the area P_τ of the τ_w incidence region were carried out for four angular positions of the nozzle. These angles ε were respectively 30°, 45°, 60°, and 90° (Fig. 3c).
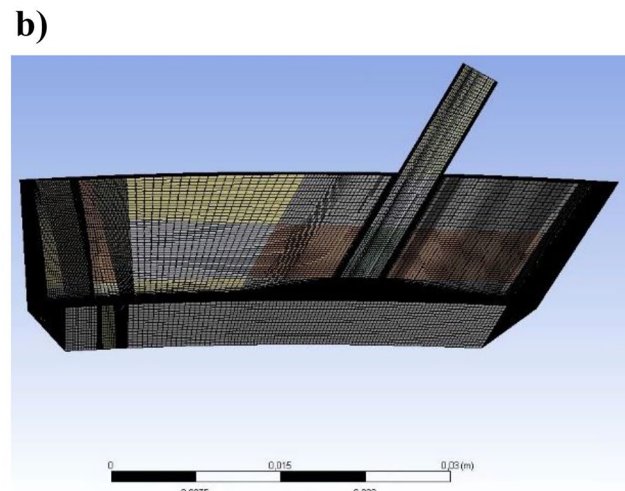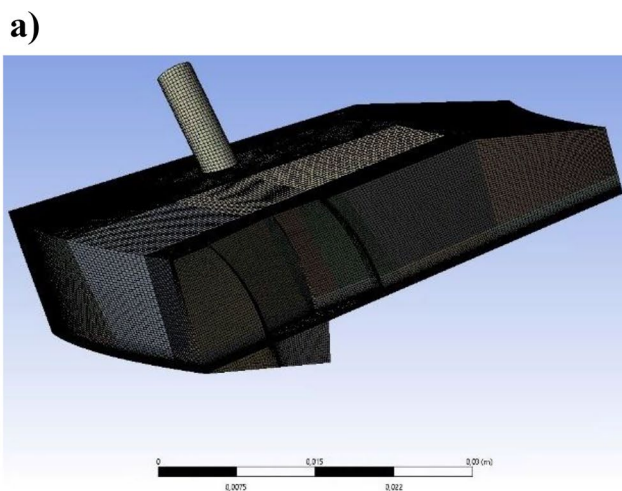
a)

b)

Fig. 5 Discrete model of the fluid domain: **a** general view and **b** cross-section

Table 3 Characteristics of conditions of simulations

Software	ANSYS CFX 2019			
Assumptions	Only the rotational movement of the grinding wheel was taken into account			
	Air has the properties of an excellent gas			
	All walls were modeled as smooth			
Simplifications	Feed movements were omitted in order to simplify the system kinematics and shorten the time of simulation calculations			
	The number of geometric variants of the simulation was limited to four nozzle inclination angle settings ε: 30°; 45°; 60°, 90°			
	The influence of earth acceleration on the flow of factors in the system under consideration was omitted			
	Heat exchange was omitted			
Geometric parameters of the model	The geometric parameters of the 3D CAD model are listed in Table 1			
Finite element mesh parameters	30°	45°	60°	90°
	5,120,877 nodes	3,115,011 nodes	2,119,321 nodes	2,346,014 nodes
	5,449,291 elements	3,462,537 elements	2,110,772 elements	2,598,229 elements
Properties of the fluid used in the simulation	Air	Model: ideal gas from the ANSYS® library		
		Morphology: fluid in continuous phase		
Conditions of the simulation process	Type of analysis: steady state			
	Continuous phase turbulence model: shear stress transport (SST) model with Kato and Launder's modification			
	Reference pressure value: 1013 hPa			
	Gravity influence model: no gravity influence			
	Degree of turbulence intensity: average (intensity 5%)			
	Flow condition: subsonic			
	Air supply speed: 50 m/s			
	Grinding wheel rotational speed: $n_s = 2950$ rpm, clockwise			
	Wall condition: no slip wall			
	Air temperature: -20 ℃			

It was assumed that the surface to be used in order to determine what part of the nominal air flow passes through the exit surface from the fluid domain was located under the hob cutter tooth shown in Fig. 6. It should be mentioned that, for the purpose of this simulation, a simplification was made by assuming that the hob gear and the grinding wheel are stationary with respect to each other except for rotation of the grinding wheel with a rotational speed $n_s = 2950$ rpm. This simplification

Fig. 6 Inflow and outflow surface of the fluid domain (red)

results from the fact that during machining, the length of the contact line between the grinding wheel and the contact surface of the hob cutter, which has the shape of a cog, changes continuously and, consequently, the size of the exit surface from the fluid domain would also change. According to the authors, failure to adopt this simplification would lead to an unnecessary increase in numerical simulation time.

Finally, the efficiency η_{ws} was defined as the ratio of the mass flow $\dot{m}_{in}$ of air at the inlet surface into the fluid domain to the mass flow $\dot{m}_{out}$ of air at the outlet surface from the fluid domain:

$$\eta_{ws} = \frac{\dot{m}_{in}}{\dot{m}_{out}} \tag{1}$$

The numerical simulations were carried out using Ansys CFX 2019 software. The initial and boundary conditions were defined as.

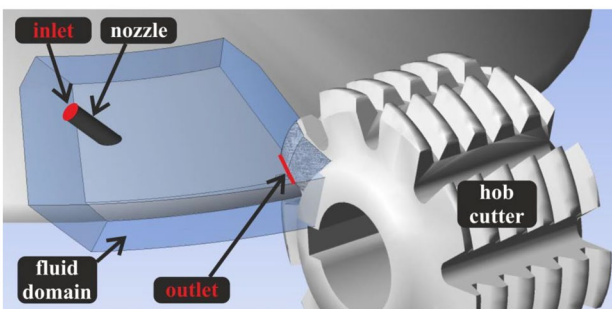– working medium: air (air model—ideal gas—was used in the CFX program);

– velocities at the nozzle inlet: 50 m/s (value for WNT nozzle determined by anemometer measurement);
– rotational speed of grinding wheel conical surface $n_s = 2950$ rpm, clockwise.

For the purpose of the simulation, it was assumed that the absolute atmospheric pressure was 1013 hPa. Relative to this, the value of the pressure at the exit surfaces from the fluid domain was defined as 0 Pa.

2.3.3 Turbulence model

A review of the literature [67–71] indicates that a properly chosen RANS turbulence model using Reynolds-averaged Navier–Stokes equations should correctly predict the effect of small vortex structures on the overall simulated flow and calculate reliable averaged values of the simulated flow parameters.

In the present study, the "SST k-ω" model, available in Ansys CFX software [72], was used. This model is a hybrid combining the best properties of the "k-ω" and "k-ε" models and allows the introduction of a segment limiting the overproduction of turbulence kinetic energy in areas of large pressure gradients. The equations of the "k-ω" model are used to model turbulent flow in the boundary layer. Since the "k-ω" model is very sensitive to the values of turbulent quantities in free flow, it is replaced by the "k-ε" model in layers further from the wall. This model simulates turbulence in free flow well and is less sensitive to inlet conditions for the quantities describing turbulence. The desirable features of both models are combined into a single model using the fact that the standard "k-ε" model can be transformed into equations for k and ω due to the fact that ω is the inherent kinetic energy dispersion of turbulence; thus, $\omega = \varepsilon / k$. The equations of this model are then multiplied by a function which has a value of 1 in free flow and 0 at the wall, while the equations of the standard "k-ω" model are multiplied by the F_1 function. The model, through the equation for turbulent viscosity, limits the values of the flow principal stresses. The model equations used are as follows:

– turbulent kinetic energy:

$$\frac{\partial(\rho k)}{\partial t} + \frac{\partial\left(\rho u_j k\right)}{\partial x_j} = -P - \beta^* \rho \omega k + \frac{\partial}{\partial x_j}\left[\frac{\left(\mu + \sigma_k \mu_t\right)\partial k}{\partial x_j}\right]$$

(2)

– dissipation of turbulent kinetic energy:

$$\frac{\partial(\rho \omega)}{\partial t} + \frac{\partial\left(\rho u_j \omega\right)}{\partial x_j} = -\frac{\gamma}{v_t}P - \beta^* \rho \omega^2 + \frac{\partial}{\partial x_j}\left[\left(\mu + \sigma_\omega \mu_t\right)\frac{\partial \omega}{\partial x_j}\right]$$
$$+ 2\left(1 - F_1\right)\frac{\rho \sigma_{\omega 2}}{\partial \omega}\frac{\partial k}{\partial x_j}\frac{\partial \omega}{\partial x_j}$$

(3)

where

– turbulent viscosity

$$v_t = \frac{a_1 k}{\max(a_1 \omega, SF_2)}$$

(4)

– production term

$$P = \mu_t SS$$

(5)

whereby

$$S = \sqrt{\frac{1}{2}\left(\frac{\partial u_i}{\partial x_j} + \frac{\partial u_j}{\partial x_i}\right)^2}$$

(6)

– functions F1 and F2:

$$F_1 = \tanh\left(\arg_1^4\right), \arg_1 = \min\left(\max\left(\frac{\sqrt{k}}{0.09\omega y}, \frac{500\nu}{\omega y^2}\right), \frac{4\rho\sigma\omega^2 k}{CDk\omega y^2}\right)$$

(7)

$$F_2 = \tanh(\arg_2^2), \arg_2 = \max\left(2\frac{\sqrt{k}}{0.09\omega y}, \frac{500\nu}{y^2\omega}\right)$$

(8)

– fixed coefficients

$$\sigma_{k1} = 0.85 \sigma_{\omega 1} = 0.5 \beta_1 = 0.075 \beta^* = 0.09 \kappa = 0.41 \gamma_1 = \frac{\beta_1}{\beta^*} - \sigma_{\omega 1}\kappa^2\sqrt{\beta^*}$$

$$\sigma_{k2} = 1.0 \sigma_{\omega 2} = 0.856 \beta_2 = 0.0828 \beta^* = 0.09, \kappa = 0.41 \gamma_2 = \frac{\beta_2}{\beta^*} - \sigma_{\omega 2}\kappa^2\sqrt{\beta^*}$$

2.3.4 Modification of the production conditions

In the "SST k-ω" model, Kato-Launder modifications [73] were applied. Normally, the "SST k-ω" turbulence model tends to artificially overproduce turbulence in the pile-up regions due to the large S values that are generated in these regions. Kato-Launder's proposal is to replace shear stress S in the turbulence production equation by vorticity Ω, then

$$P = \mu_t S\Omega$$

(9)

where

$$\Omega = \sqrt{\frac{1}{2}\left(\frac{\partial \mathrm{u}_i}{\partial x_j} - \frac{\partial \mathrm{u}_j}{\partial x_i}\right)^2} \qquad (10)$$

2.3.5 Wall shear stresses on the grinding wheel surface

Due to the shear effect in the abrasive layer [74, 75], the wall shear stress τ_w occurring on the conical surface of the grinding wheel (wall) was used in the analysis of numerical simulations in order to determine the possibility of removing contaminants from the grinding wheel active surface by use of the CCA jet. These stresses are described by the formula

$$\tau_w = \mu \left(\frac{\partial u}{\partial y}\right)_{y=0} \qquad (11)$$

where τ_w is the shear stress on the conical surface of the grinding wheel (wall), μ is the dynamic viscosity, u is the velocity over the conical grinding wheel surface (wall), and y is the distance from the wall of the conical grinding wheel surface.

2.3.6 Conditions of the numerical simulations

ANSYS CFX 2019 software was used to carry out the numerical simulations of the flow, using a 3D CAD model whose geometric parameters are described in Table 1. Table 3 summarizes the conditions applied during the numerical work carried out. Among other things, the

assumptions and simplifications made are listed, as well as the parameters of the finite element mesh. Furthermore, the properties of the fluid used and the conditions of the simulation process are listed.

Mesh convergence analysis was carried out by incrementally increasing the number of elements and verifying the estimations to ensure convergence of the numerical solution. The chart in Fig. 7 shows that for each of the four geometric variants differing in the angular position of the nozzle, the densification of the grid causes the results to converge around a single value. The fact that the efficiency η_{ws} for each of the four variants is lower with lower mesh densification is due to the fact that in the gap between the abrasive tool and the workpiece, the geometry of the closely spaced walls is reproduced incorrectly and the calculations in the wall layer erroneously reduce the amount of fluid that enters this area. By properly densifying this area and the area around the main fluid stream, it is possible to achieve a plateau in the η_{ws} efficiency results.

3 Results of numerical simulations of compressed cold air flow in grinding zone of hob cutter blades using CAG nozzle

3.1 Efficiency η_{ws} of air supply system

Figure 8 shows the distribution of air flow streamlines in the fluid domain obtained by numerical simulation for four nozzle angle settings: 30°, 45°, 60°, and 90°.

Fig. 7 Mesh independence study
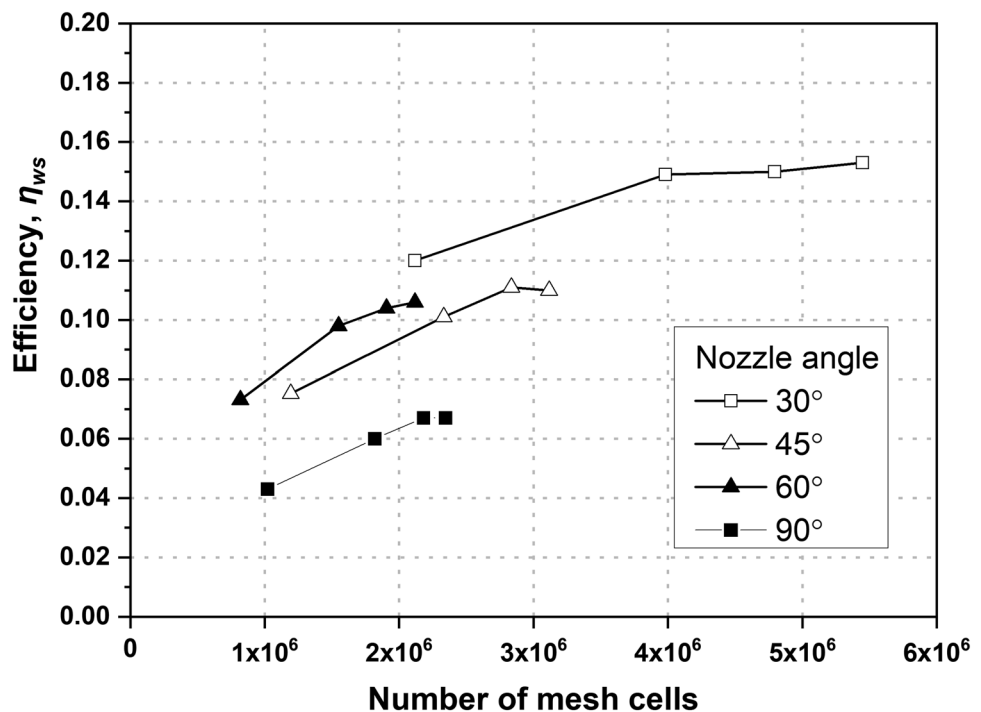
As can be observed in Fig. 8, decreasing the angle ε of inclination of the nozzle in relation to the grinding wheel active surface causes the lines representing air streams to be more directed and directed "under the tooth" of the hob cutter (opposite to the direction of rotation of the grinding wheel). This results in a greater volume of air flow reaching the contact zone of the hob cutter with the grinding wheel due to lower losses resulting from multidirectional dispersion of air flow from the point of contact with the rotating grinding wheel surface, which occurs when the nozzle is inclined at an angle of 90°, for instance (Fig. 8d).

A confirmation of the above-described effect of changes in the inclination angle ε on the directionality of the CCA jet is provided by the results of efficiency η_{ws}, which defines the ratio of the amount of air delivered by the nozzle to the grinding zone to the amount of air entering directly into the zone of contact between the grinding wheel and the hob cutter. The results are summarized in Table 4 and shown in Fig. 9.

As can be seen from the data in Table 4 and Fig. 9, decreasing the angle ε increases the efficiency of CCA supply to the grinding zone expressed as η_{ws} efficiency. The highest efficiency η_{ws}, i.e., the most favorable from the point of view of cooling and cleaning of the grinding zone, was achieved when the nozzle was positioned at an angle $\varepsilon = 30°$ with respect to the grinding wheel active surface. It should be noted that in the case of two successive angular settings of the nozzle (45° and 60°), the efficiency achieved for them reaches almost identical values, but is lower than the highest one by about 30%. Such a large difference in the values obtained is due to the nature of the flow. The numerical simulation indicates that at a nozzle inclination of 30° in relation to the GWAS, the air stream, due to the presence of an air cushion around the rotating grinding wheel, does not reach the GWAS for the most part. Thus, it is not dispersed as a result of contact with the grinding wheel and is directed directly to the point of contact between the grinding wheel and the hob cutter.
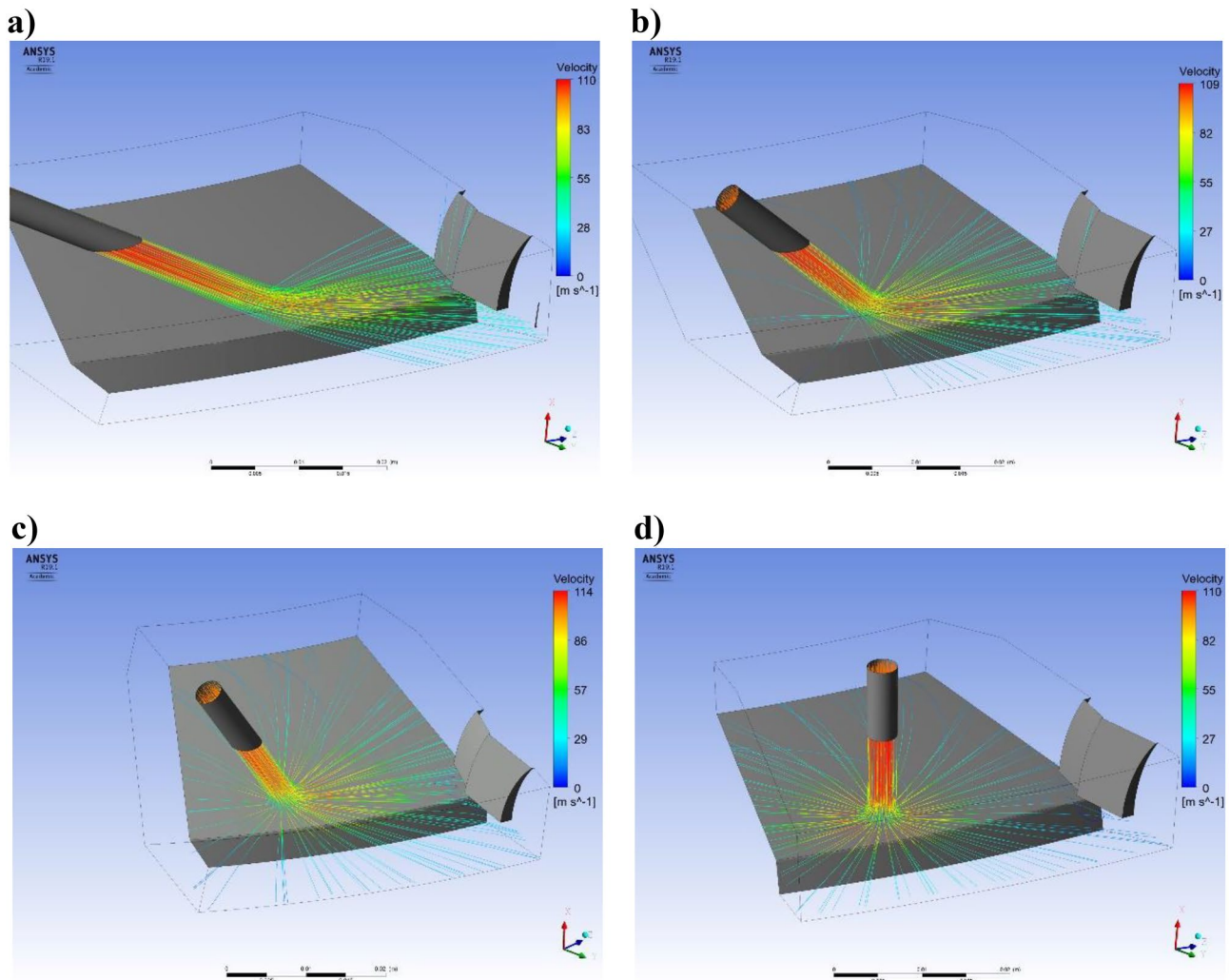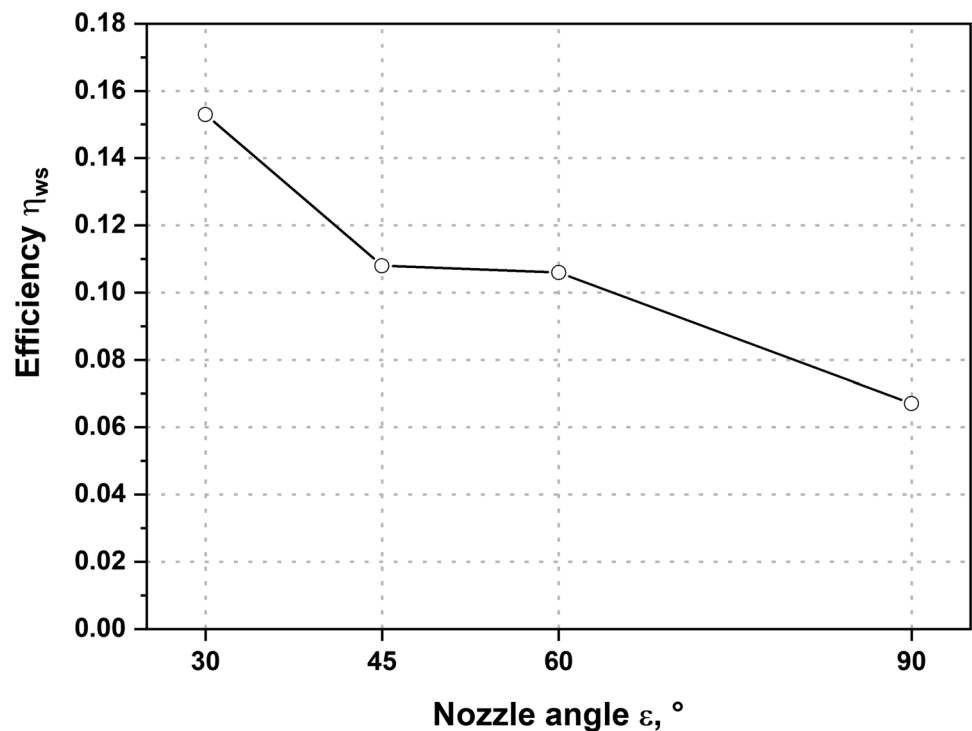

Fig. 8 Velocity vector distribution on the current line obtained for the angle ε of the nozzle inclination: **a** 30°, **b** 45°, **c** 60°, and **d** 90°

Table 4 Efficiency η_{ws} of air supply system using CCA method

Nozzle inclination angle ε [°]			
30	45	60	90
Efficiency η_{ws} [−]			
0.153	0.108	0.106	0.067

In comparing the above-mentioned values of efficiency with the values obtained using the MQL method (described by the authors in [40]), it should be noted that the efficiency of the air supply system obtained for identical angles of nozzle inclination in both cases changes in an analogous way – for $\varepsilon = 30°$ it takes on the highest value, while for $\varepsilon = 90°$ it is the lowest. Nevertheless, it should be noted that the efficiency values obtained for the MQL method are 90–160% higher than the corresponding values obtained for the CCA method. It must be assumed that this is due to the way the nozzle is positioned with respect to the direction of rotation of the grinding wheel. In the case of the MQL method, the air stream leaving the nozzle encounters an air cushion around the rotating grinding wheel in a clockwise direction. As a result, it is lifted by the air cushion and directed directly to the point of contact between the grinding wheel and the hob cutter. When a CAG nozzle is used, the clockwise rotation of the grinding wheel impedes air flow to the contact area between the grinding wheel and the hob cutter.

3.2 Wall shear stress τ_w and area P_τ of action of wall shear stress τ_w

Figure 10 shows the distributions of the wall shear stress τ_w occurring on the conical surface of the grinding wheel in the area of the active surface of the wheel. The distributions are shown for four nozzle angle settings, namely, 30°, 45°, 60°, and 90°.

Table 5 and Fig. 11 show the maximum wall shear stress $\tau_{w\text{-max}}$ values obtained for nozzle inclination angles ε of 30°, 45°, 60°, and 90°, respectively.

From the data in Table 5 and Fig. 11, it can be concluded that the highest value of wall shear stress occurs when the CAG nozzle is set at an angle $\varepsilon = 90°$, similar to the authors' study on air utilization using the MQL method [40]. Moreover, as the angle of inclination of the CAG nozzle decreases, the wall shear stress τ_w also decreases and reaches, for an angle $\varepsilon = 30°$, a $\tau_{w\text{-max}}$ value less than half the value obtained for an angle $\varepsilon = 90°$. This results from the already mentioned occurrence of the air cushion around the rotating grinding wheel, which causes that the smaller the value of the nozzle inclination angle, the less air reaches the GWAS, while more enters the contact zone between the grinding wheel and the hob cutter.

It should be noted that the ability to remove contaminants from the active surface of the grinding wheel is also influenced, apart from the value of wall shear stress τ_w, by the
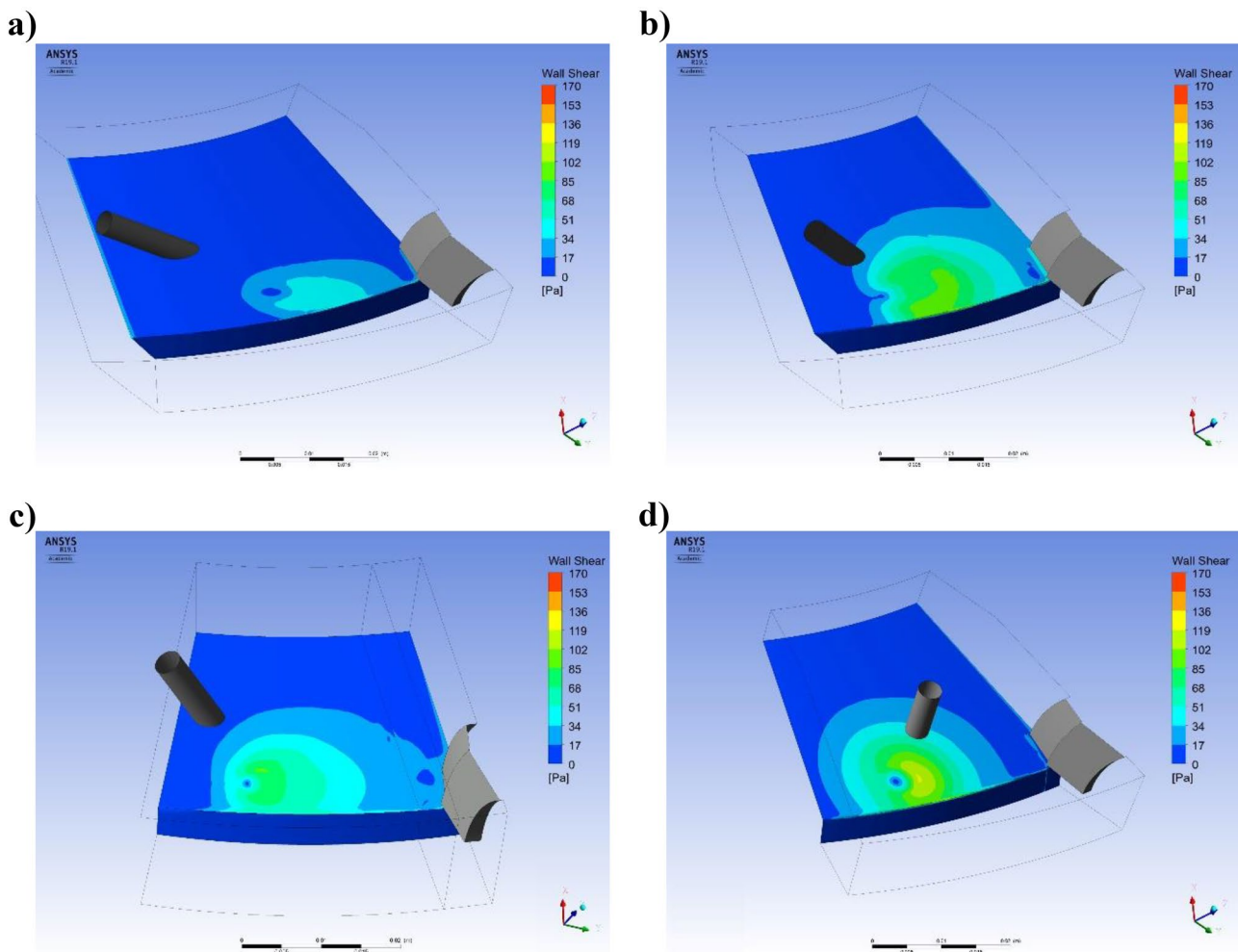
Fig. 9 Efficiency η_{ws} of CCA air supply system obtained for four angles ε of nozzle inclination, namely, 30°, 45°, 60°, and 90°

Fig. 10 Distribution of wall shear stress τ_w obtained for angle ε of nozzle inclination: **a** 30°, **b** 45°, **c** 60°, and **d** 90°

area P_τ on which these stresses act. The greater the surface area P_τ, the greater the ability to remove contaminants from the grinding wheel surface. Table 6 summarizes the values of the surface area P_τ of the action of wall shear stress τ_w induced by the CCA jet, determined for four cases of nozzle angular settings ($\varepsilon = 30°$, 45°, 60°, and 90°). For each of the four angles ε, the area is defined by three intervals of wall shear stresses with values of (1) 30–170 Pa, (2) 40–170 Pa, and (3) 50–170 Pa.

To illustrate the shape and size of the P_τ area obtained as a function of the nozzle inclination angle ε, they are summarized in Fig. 12. This figure shows the P_τ area obtained
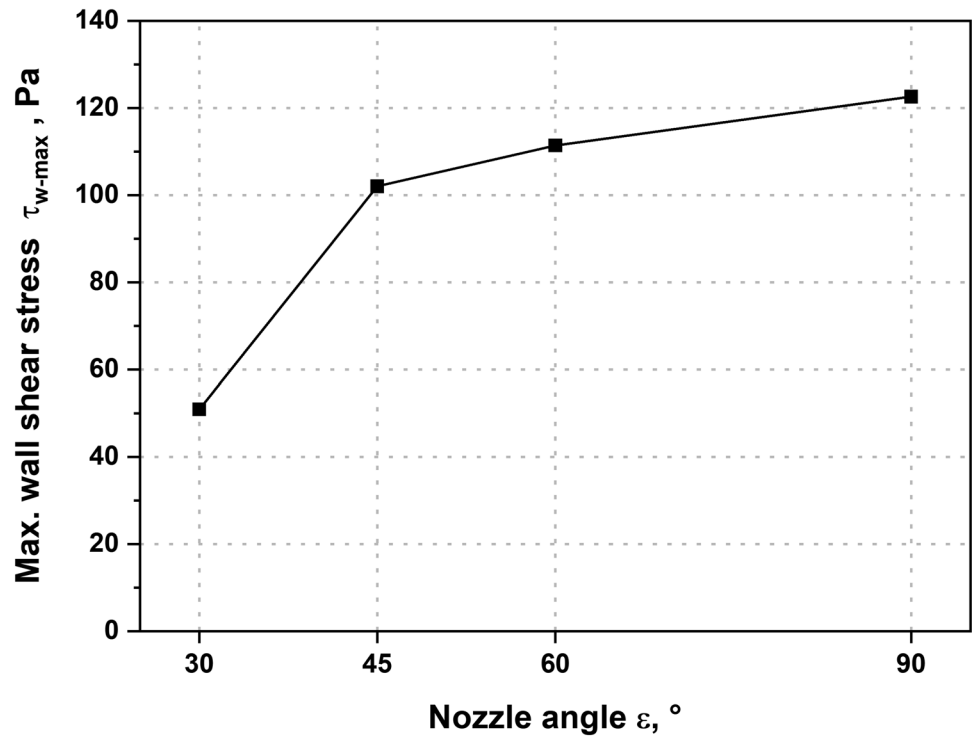
for case 1, when the wall shear stress τ_w is between 30 and 170 Pa. The surface area is marked in green.

In order to facilitate the analysis of the results in Table 6, their values were used to make the graph shown in Fig. 13.

From Table 6 and Fig. 13, it can be seen that for all three ranges of τ_w, the largest P_τ surface area was obtained when the nozzle was positioned at an angle $\varepsilon = 45°$ to the grinding wheel active surface. Similarly, although smaller on average by about 5.9%, values were obtained when the nozzle was positioned in a direction normal ($\varepsilon = 90°$) to the GWAS. When an angle of $\varepsilon = 60°$ was used, the difference averaged 16.2%.

Of note is the large difference (about 215 mm^2 on average) in the P_τ values obtained for the cases when the nozzle is positioned at 30° and 45°. Such a large difference results from the nature of the flow and is caused by the occurrence of an air cushion around the rotating grinding wheel, which blocks most of the air stream from reaching the GWAS, a fact that was mentioned when discussing

Table 5 Maximum wall shear stress $\tau_{w\text{-max}}$

Nozzle inclination angle ε [°]			
30	45	60	90
Maximum wall shear stress $\tau_{w\text{-max}}$ [Pa]			
50.9	102.0	111.4	122.9

Fig. 11 Maximum wall shear stress $\tau_{w\text{-max}}$ obtained for four angles ε of nozzle inclination: 30°, 45°, 60°, and 90°

4 Experimental verification of numerical simulation results

4.1 Grinding of face of hob cutters

The aim of the experimental study was to verify the results of numerical simulations of compressed cold air (CCA) flow in the grinding zone. The amount of clogging occurring on the grinding wheel active surface was selected as the parameter verifying the efficiency of the air supply. This is due to the fact that one of the functions of the cooling lubricant is to remove the swarf from the grinding zone and to clean the wheel.

In the course of experimental investigations, the contact surface of a hob cutter was ground, and then the surface

Table 6 Surface area P_τ of wall shear stress τ_w

Wall shear stress τ_w [Pa]	Nozzle inclination angle ε [°]			
	30	45	60	90
	Surface area P_τ [mm^2]			
30–170	95.0	334.0	285.5	313.1
40–170	29.7	251.3	209.4	232.9
50–170	0.3	189.5	157.2	181.9

the efficiency diagram η_{ws} in Fig. 9 and the diagram of maximum wall shear stress $\tau_{w\text{-max}}$ (Fig. 11).

proportion of deposits on the active surface of the wheel was measured. It was on this basis that a percentage index $Z_\%$ of the grinding wheel cloggings was determined. The obtained results allowed an indirect evaluation of the air supply conditions in the CCA method determined by the angle ε of inclination of the CAG nozzle.

During grinding, the face of solid hob cutters NMFc-3/20°/B, made of HS6-5–2 high-speed steel without anti-wear coatings, was sharpened. These cutters are designed for the production of cylindrical gears according to ISO 53 and ISO 54. Table 7 summarizes the grinding conditions used during the described tests.

The cutters were sharpened on a special conventional grinding machine for sharpening hob cutters using a Norton 38A60KVBE disc wheel [65]. This is a grinding wheel made of white fused alumina grains with a vitrified bond. The wheel was conditioned before each test using a single-grain diamond dresser. The grinding parameters for the hob cutter blades were selected based on literature data [76, 77] and workshop practice.

During the first stage of the research, compressed cold air (CCA) was applied using a single CAG nozzle with the symbol WNT 6910.15.3–7. The nozzle was inclined with respect to the active surface of the grinding wheel using four angles ε amounting to 30°, 45°, 60°, and 90°. As a reference, machining was also carried out with the minimum quantity of machining fluid using the MQL method. In this method, coolant in the form of an air-oil aerosol was supplied using a MicroJet MKS-G100 MQL system from MicroJet
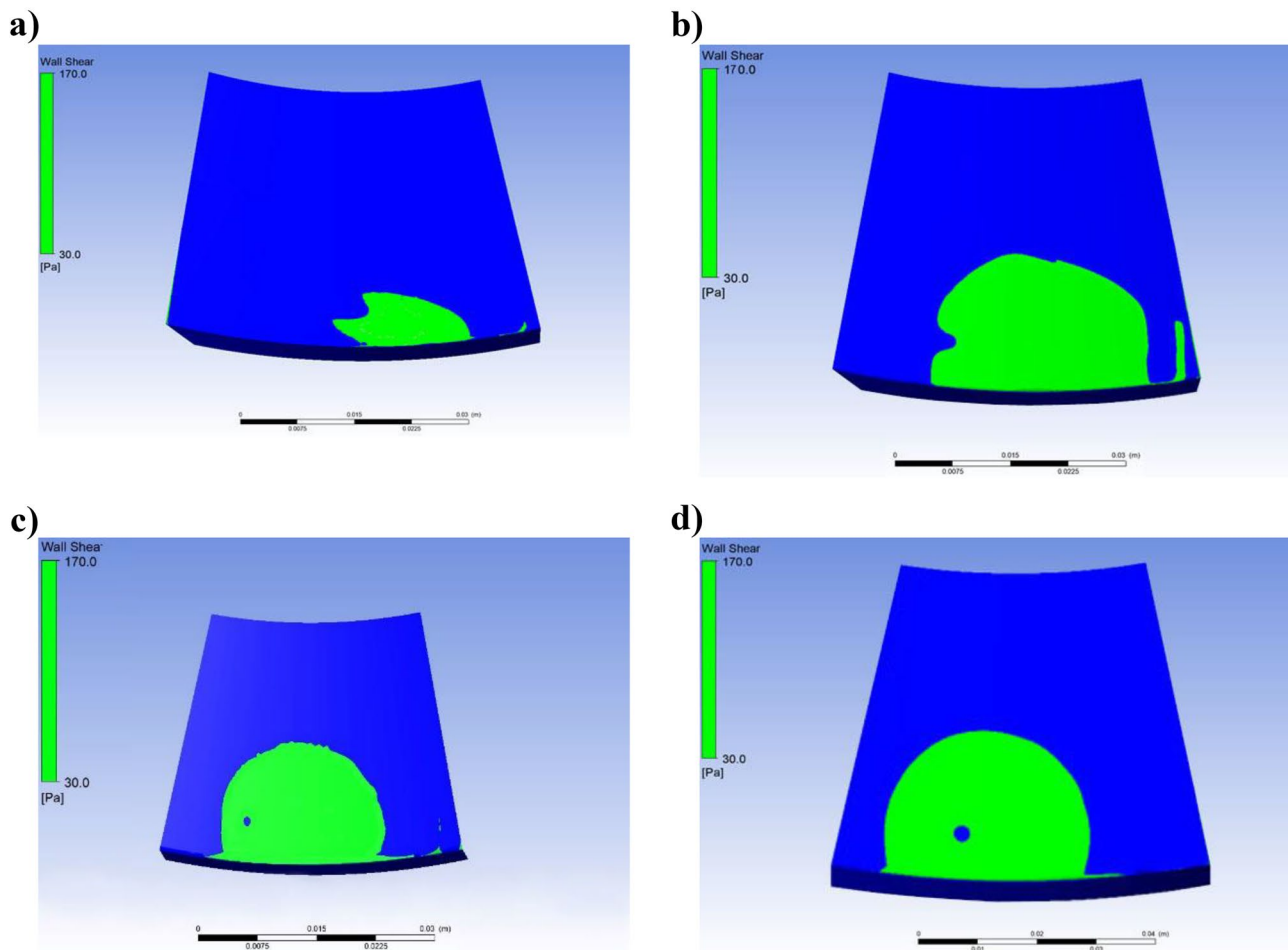
Fig. 12 Area P_τ of occurrence of wall shear stress τ_w in the range 30–170 Pa obtained for angles ε of nozzle inclination: **a** 30°, **b** 45°, **c** 60°, and **d** 90°

(Germany) with a flow rate of $Q_{MQL}=50$ ml/h. Biocut 3000 synthetic ester-based oil from Molyduval (Germany) was used as the liquid [78]. The nozzle was an inclined relative of the grinding wheel active surface using four ε angles of 30°, 45°, 60°, and 90°. The air-oil aerosol supply conditions were determined based on previous studies described in detail in [40].

In the second stage of the experimental study, the grinding of the hob cutter face was carried out using the MQL-CCA method and the flood (WET) method. During machining with the MQL-CCA method, the machining conditions adopted in the first stage of the research were applied during individual trials for each method. The exception was the variant in which the nozzles were positioned at an angle ε that allowed the lowest $Z_\%$ to be obtained. In the case of the nozzle used in the MQL method, this was an angle $\varepsilon=90°$, while in the case of the CCA method, the angle ε was 45°. The flood method (WET) was carried out using an

aqueous oil emulsion with Emulgol ES-12 (5%) from Orlen Oil (Poland) [79]. The emulsion supply conditions to ensure the lowest index of wheel flooding were established based on previous studies [55]. A single nozzle inclined with respect to the active surface of the wheel by an angle $\varepsilon=30°$ was used, which supplied the emulsion to the grinding zone at a nominal flow rate $Q_{WET}=7$ l/min.

4.2 Conditions for grinding wheel clogging measurements

Measurements of wheel bonding were commenced by recording images of a fragment of the grinding wheel active surface (GWAS) using a digital microscope DO Smart 5MP PRO from Delta Optical (Poland) [80]. The images were recorded using Delta Optical Smart Analysis 1.0.5 software using 50× magnification (Fig. 14a). Images recorded in grayscale were analyzed to detect the occlusions and

Fig. 13 Area P_τ of occurrence of wall shear stress τ_w obtained for three ranges of stress values, namely, 30–170 Pa, 40–170 Pa, and 50–170 Pa
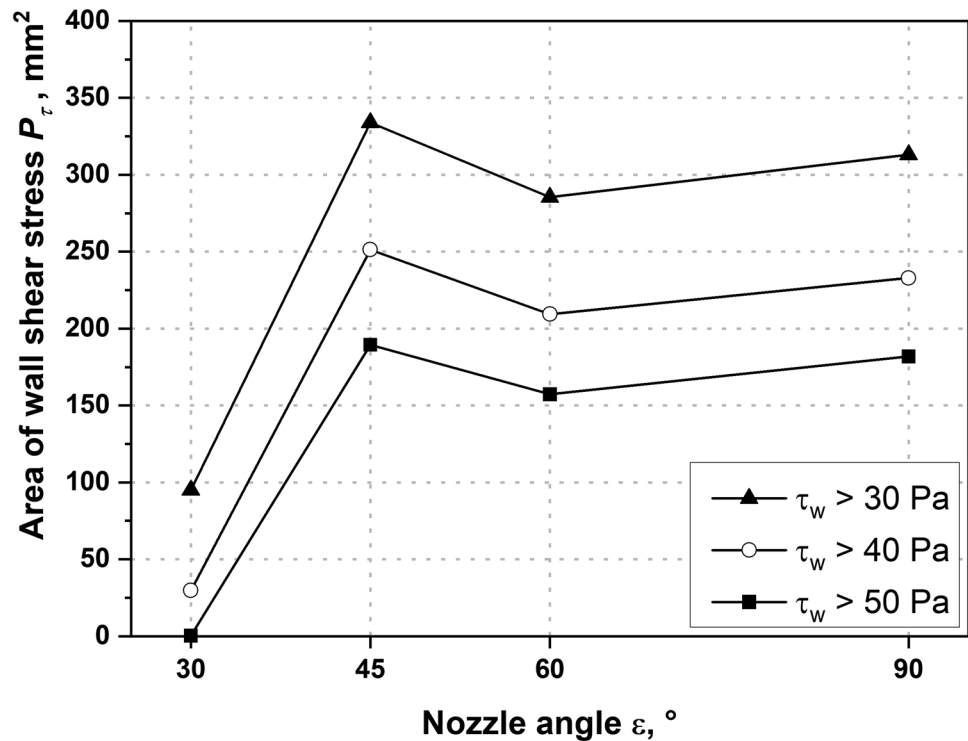
then to determine the degree of filling of the inter-grain spaces of the grinding wheel by the chips. For this purpose, the Met-Ilo v.5.1 image analysis program developed at the Silesian University of Technology [81] was used. This program enables the detection of chips accumulated between the abrasive grains on the basis of the intensity of the light reflected from the chips in relation to the intensity of the light reflected from the surface devoid of them. This difference in reflected light intensity is used to segment the image area by setting the color of the pixels corresponding to the chips as white and giving the remaining pixels a red color (Fig. 14b). As a result of dividing the number of black pixels by the total number of pixels, the grinding wheel clogging index $Z_\%$ was determined. The final value of the $Z_\%$ index of grinding wheel clogging representative for a single grinding trial was determined as the arithmetic mean of the index values determined from five GWAS images taken at different locations on the circumference of the grinding wheel and in total covering approximately 6% of the GWAS area [55].

4.3 Experimental results and their analysis

Table 8 and Fig. 15 show the results of the measurement of the active surface indentation of the grinding wheel during grinding with a stream of compressed cold air (CCA) and coolant supplied at a minimum flow rate using the MQL

method. The percentage of surface clogging on the GWAS is described by the $Z_\%$ index of grinding wheel clogging.

As can be seen from Table 8 and Fig. 15, when the CAG nozzle is used, the $Z_\%$ index assumes the smallest (most favorable) value for the nozzle inclination angle $\varepsilon = 45°$ and increases its value for the other angle settings. This character of the occurrence of clogging coincides with the values obtained from numerical simulations described in "Sect. 2." The smallest percentage of cloggings on the GWAS observed at a CAG nozzle inclination of $\varepsilon = 45°$ is mainly due to the largest surface area P_τ, which is affected by the second highest wall shear stress τ_w induced by the CCA jet. Moreover, the cleaning effect of the grinding wheel is enhanced by the air jet directed into the contact zone of the active abrasive grains with the workpiece material, as confirmed by the second highest value of the efficiency η_{ws} of the air supply system.

In the case of the results obtained for the MQL method, the $Z_\%$ index takes the smallest (most favorable) value for the nozzle inclination angle $\varepsilon = 90°$. It should be noted here that the values of the $Z_\%$ index obtained for the other angles ε are similar. The difference between the extreme $Z_\%$ values obtained for the angle $\varepsilon = 30°$ and $\varepsilon = 90°$ is only 2.3%. Therefore, it can be concluded that a change in the angle ε does not have a significant effect on the efficiency of chip removal from the inter-grain spaces of the grinding wheel. This property can be explained by analyzing the results of numerical simulations and assuming that the

Table 7 Grinding conditions

Grinding mode	Hob resharpening
Grinding machine	Conventional hob grinding machine

Workpiece	Hob cutter NFMc-3/20°/B
	  material: HS6-5–2 high-speed steel, hardened with 62 ± 1 HRC
	  $m = 3$ mm
	  $\alpha = 20°$
	  $z_h = 9$
	  accuracy class: B (according to PN-ISO 4468)
	  normal ground profile

Grinding wheel	38A60KVBE
	  dish grinding wheel – type 12 (according to PN-ISO 525:2001)
	  dimensions: $200/90 \times 20/2 \times 32$

Dressing parameters	Single-point diamond dresser $Q_d = 1.0$ kt

Grinding parameters	$n_s = 2950$ rpm
	  $v_s = 31$ m/s
	  $v_w = 6.6$ m/min
	  $a = 0.15$ mm
	  $a_e = 0.01$ mm
	  15 grinding passes

Method of coolant supply	1. Compressed cold air method (CCA)
	  WNT 6910.15.3–7 – cold air gun (CAG) with single nozzle
	  $p_{CCA} = 0.6$ MPa
	  $T_{CCA} = -20$ ℃
	  $\varepsilon = 30°, 45°, 60°, 90°$
	2. Minimal quantity lubrication method (MQL)
	  MicroJet MKS-G100 – oil-mist generator with single external nozzle
	  Fluid: Biocut 3000
	  $Q_{MQL} = 50$ ml/h
	  $\varepsilon = 30°, 45°, 60°, 90°$
	3. MQL-CCA – combined MQL and CCA method
	  CCA method: $\varepsilon = 45°$
	  MQL method: $\varepsilon = 30°$
	4. Flood method (WET)
	  Fluid: 5% water solution of Emulgol ES-12 oil
	  $Q_{WET} = 7$ l/min
	  $\varepsilon = 30°$

influence of air entering the contact zone of the workpiece/wheel (expressed by the efficiency η_{ws}) on grinding wheel clogging is equivalent to the influence of the wall shear stress τ_w acting on the GWAS [40]. For an angle $\varepsilon = 90°$, the wall shear stress τ_w has a decisive influence on the GWAS

cleaning. With decreasing the nozzle inclination angle, the influence of τ_w stresses also decreases, and the cleaning function is taken over by the air entering directly into the contact zone of the grinding wheel with the attack surface of the sharpened hob cutter.

Fig. 14 Measurements of bonding of grinding wheel: **a** GWAS photo after grinding, magnification $50\times$; **b** GWAS photo processed to determine $Z_\%$
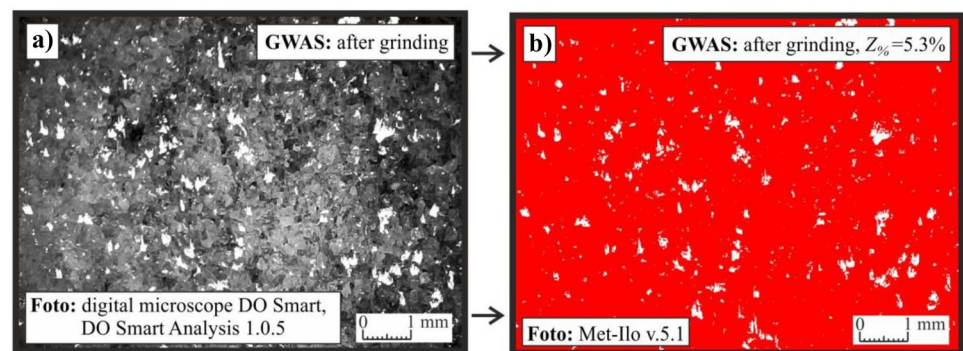
Table 8 $Z_\%$ index of clogging for CCA and MQL

Method of coolant supply	Nozzle inclination angle ε [°]			
	30	45	60	90
	Grinding wheel clogging coefficient $Z_\%$ [%]			
CCA	12.5	5.3	10.5	15.9
MQL	15.8	14.3	15.1	13.5

Table 9 Lowest values of $Z_\%$ index for CCA, MQL, MQL-CCA, and WET methods

Method of coolant supply			
CCA	MQL	MQL-CCA	WET
Grinding wheel clogging index $Z_\%$ [%]			
5.3	13.5	2.5	2.0

A comparison of the $Z_\%$ values obtained during grinding using the CCA method and the MQL method indicates a much better cleaning ability of compressed cold air at an angular position of the CCA nozzle in the range from 30 to 60°. The difference between the best $Z_\%$ values obtained for both methods is 8.2%, with the $Z_\%$ value for the MQL method being 2.5 times higher than that for the CCA method.

Table 9 and Fig. 16 summarize the results of the most favorable (smallest) values of the $Z_\%$ index of wheel clogging determined for four methods of supplying machining fluid to the grinding zone: CCA, MQL, MQL-CCA, and WET.

As can be seen from the analysis of the results presented above, the smallest value of the $Z_\%$ index was obtained by supplying the cooling lubricant using the flood method (WET). The application of an additional GWAS cleaning

nozzle using compressed cold air (CCA) and supporting the MQL method resulted in the $Z_\%$ value determined for the hybrid MQL-CCA method being higher by a mere 0.5% in comparison with the indicator for the priming method (WET).

The above observations and the fact that the $Z_\%$ value for the MQL method is almost seven times higher than the value of the index determined for the flood method (WET) give rise to the conclusion that the function of evacuating chips from the contact zone of the GWAS with the workpiece surface and cleaning the GWAS during grinding with the MQL method can be effectively supported by feeding an additional stream of CCA in the manner described in this work. This makes it possible to achieve a level of wheel clogging similar to that achieved when feeding a water-in-oil emulsion using the flood method (WET) at an 8400-fold reduction in coolant output.

Fig. 15 Grinding wheel clogging index $Z_\%$ for CCA and MQL methods
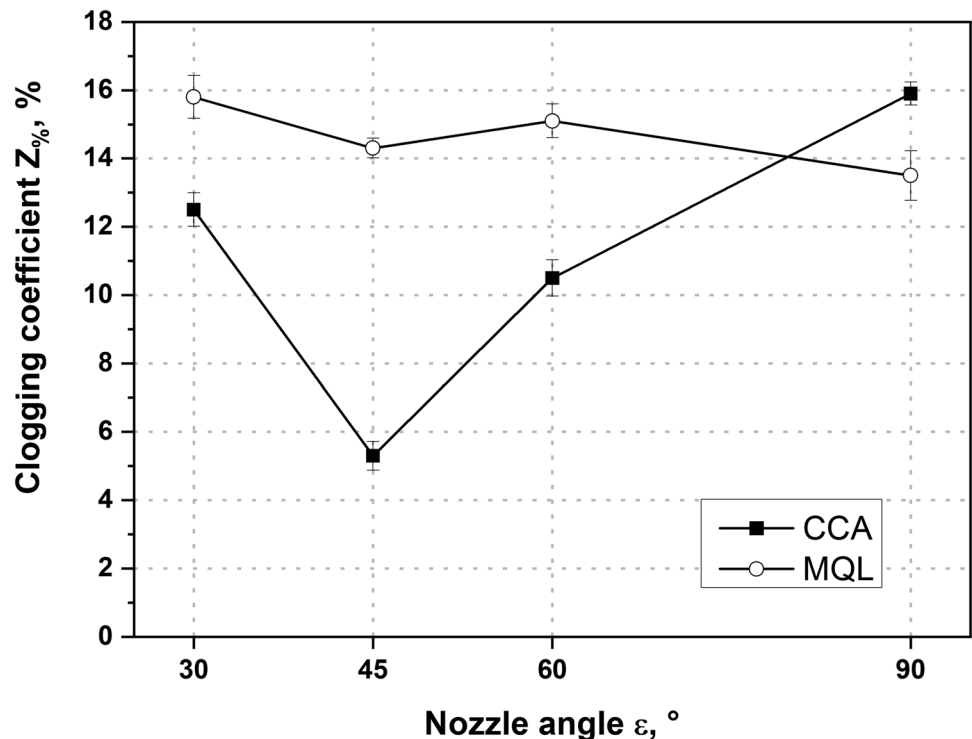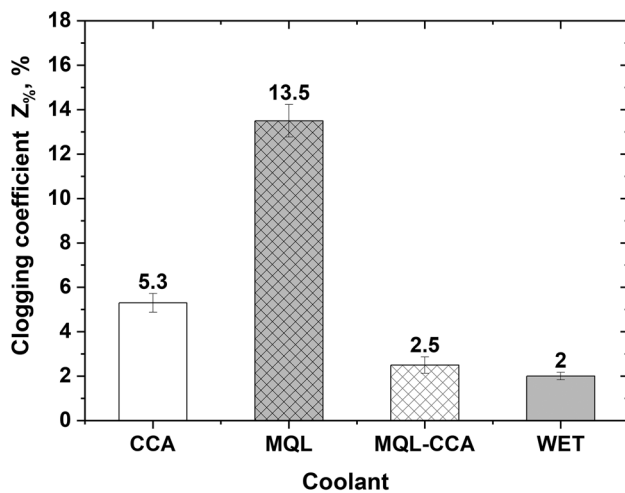
Fig. 16 Smallest values of $Z_\%$ index of grinding wheel clogging for CCA, MQL, MQL-CCA, and WET methods

5 Conclusions

By carrying out numerical flow simulations and verification experimental studies, it was established that the ability of the CCA jet to clean GWAS depends primarily on the value of the tangential shear stress τ_w and the surface area P_τ on which it acts. The greater these two values are, the smaller (more favorable) the value reached by the grinding wheel clogging index $Z_\%$. In the presented range of test conditions, the smallest $Z_\%$ value of 5.3 was obtained with the nozzle positioned at an angle of $\varepsilon = 45°$ to the GWAS and is 2.5 times lower than the value determined for the most favorable positioning of the nozzle using the MQL method, for which $Z_\% = 13.5$. This observation indicates the validity of using the CCA jet directed at the GWAS at an angle of 45° to assist in cleaning the grinding wheel during machining with the simultaneous application of the MQL method. This is confirmed by the wheel clogging condition obtained during grinding using the hybrid MQL-CCA method, for which the $Z_\%$ is 2.5 and its value is comparable to the $Z_\% = 2.0$ – value obtained for a wheel working under cooling conditions with a water-based oil emulsion supplied by the flood method (WET).

Availability of data and material Not applicable.

Code availability Not applicable.

Declarations

Conflict of interest The authors declare no competing interests.

References

1. Abubakr M, Abbas AT, Tomaz I, Soliman MS, Luqman M, Hegab H (2020) Sustainable and smart manufacturing: an integrated approach. Sustainability 12(6):2280. https://doi.org/10.3390/su12062280
2. Almeida CMVB, Agostinho F, Huisingh D, Gianetti BF (2017) Cleaner production towards a sustainable transition. J Clean Prod 142(1):1–7. https://doi.org/10.1016/j.jclepro.2016.10.094
3. Xie W, Zhang Z, Liao L, Liu J, Su H, Wang S, Guo D (2020) Green chemical mechanical polishing of sapphire wafers using a novel slurry. Nanoscale 12:22518. https://doi.org/10.1039/d0nr04705h
4. Arsene B, Pasca Pascariu G, Sarbu FA, Barbu M, Calefariu G (2018) Green manufacturing by using organic cooling-lubrication fluids. IOP Conf Ser Mater Sci Eng 339:012001. https://doi.org/10.1088/1757-899X/399/1/012001
5. Pusavec F, Krajnik P, Kopac J (2010) Transitioning to sustainable production – part I: application on machining technologies. J Clean Prod 18:174–184. https://doi.org/10.1016/j.jclepro.2009.08.010
6. Debnath S, Reddy MM, Yi QS (2014) Environmental friendly cutting fluids and cooling techniques in machining: a review. J Clean Prod 83:33–47. https://doi.org/10.1016/j.jclepro.2014.07.071
7. Marinescu ID, Hitchiner M, Uhlmann E, Rowe WB, Inasaki I (2007) Handbook of machining with grinding wheels. CRC Press, Boca Raton
8. Klocke F (2009) Manufacturing processes 2, grinding, honing, lapping. Springer, Berlin
9. Benedicto E, Carou D, Rubio EM (2017) Technical, economic and environmental review of the lubrication/cooling systems used in machining processes. Procedia Eng 184:99–116. https://doi.org/10.1016/j.proeng.2017.04.075
10. Priarone PC, Robiglio M, Setteri L, Tebaldo V (2015) Effectiveness of minimizing cutting fluid use when turning difficult-to-cut alloys. Procedia CIRP 29:341–346. https://doi.org/10.1016/2Fj.procir.2015.02.006
11. Fratila D (2010) Macro-level environmental comparison of near-dry machining and flood machining. J Clean Prod 18:1031–1039. https://doi.org/10.1016/j.jclepro.2010.01.017
12. Pusavec F, Kramar D, Krajnik P, Kopac J (2010) Transitioning to sustainable production – part II: evaluation of sustainable machining technologies. J Clean Prod 18:1211–1221. https://doi.org/10.1016/j.jclepro.2010.01.015
13. Zhang Z, Liao L, Wang X, Xie W, Guo D (2020) Development of a novel chemical mechanical polishing slurry and its polishing mechanisms on a nickel alloy. Appl Surf Sci 506:144670. https://doi.org/10.1016/j.apsusc.2019.144670

14. Zhang Z, Cui J, Zhang J, Liu D, Yu Z, Guo D (2019) Environment friendly chemical mechanical polishing of copper. Appl Surf Sci 467–468:5–11. https://doi.org/10.1016/j.apsusc.2018.10.133

15. Zhang Z, Song Y, Xu C, Guo D (2012) A novel model for undeformed nanometer chips of soft-brittle HgCdTe films induced by ultrafine diamond grits. Scripta Mater 67:197–200. https://doi.org/10.1016/j.scriptamat.2012.04.017

16. Zhang Z, Huo F, Zhang X, Guo D (2012) Fabrication and size prediction of crystalline nanoparticles of silicon induced by nanogrinding with ultrafine diamond grits. Scripta Mater 67:657–660. https://doi.org/10.1016/j.scriptamat.2012.07.016

17. Zhang Z, Wang B, Kang R, Zhang B, Guo D (2015) Changes in surface layer of silicon wafers from diamond scratching. CIRP Ann Manuf Technol 64:349–352. https://doi.org/10.1016/j.cirp.2015.04.005

18. Wang B, Zhang Z, Chang K, Cui J, Rosenkranz A, Yu J, Lin C-T, Chen G, Zang K, Luo J, Jiang N, Guo D (2018) New deformation-induced nanostructure in silicon. Nano Lett 18:4611–4617. https://doi.org/10.1021/acs.nanolett.8b01910

19. Zhang Z, Wang X, Meng F, Liu D, Huang S, Cui J, Wang J, Wen W (2022) Origin and evolution of a crack in silicon induced by a single grain grinding. J Manuf Process 75:617–626. https://doi.org/10.1016/j.jmapro.2022.01.037

20. Zhang Z, Huang S, Wang S, Wang B, Bai Q, Zhang B, Kang R, Guo D (2017) A novel approach of high-performance grinding using developed diamond wheels. Int J Adv Manuf Technol 91:3315–3326. https://doi.org/10.1007/s00170-017-0037-3

21. Zhang Z, Cui J, Wang B, Wang Z, Kang R, Guo D (2017) A novel approach of mechanical chemical grinding. J Alloy Compd 726:514–524. https://doi.org/10.1016/j.jallcom.2017.08.024

22. Kaynak Y, Lu T, Jawahir IS (2014) Cryogenic machining-induced surface integrity: a review and comparison with dry, MQL, and flood-cooled machining. Mach Sci Technol Int J 18(2):149–198. https://doi.org/10.1080/10910344.2014.897836

23. Lawal S, Choudhury I, Nukman Y (2013) A critical assessment of lubrication techniques in machining processes: a case for minimum quantity lubrication using vegetable oil-based lubricant. J Clean Prod 41:201–221. https://doi.org/10.1016/j.jclepro.2012.10.016

24. Nadolny K, Kieraś S, Sutowski P (2021) Modern approach to delivery coolants, lubricants and antiadhesives in the environmentally friendly grinding processes. Int J Precis Eng Manuf-Green Technol 8:639–663. https://doi.org/10.1007/s40684-020-00270-y

25. Ebbrell S, Woolley NH, Tridimas YD, Allanson DR, Rowe WB (2000) The effects of cutting fluid application methods on the grinding process. Int J Mach Tools Manuf 40(2):209–223. https://doi.org/10.1016/S0890-6955(99)00060-7

26. Klocke F, Beck T (1998) Gut geschmiert statt schlecht gekühlt. Kühlschmier-stoffreduzierung beim. CBN-Hochgeschwindigkeitsschleifen. Werkstattstechnik 88(9–10):400–404

27. Madanchi N, Kurle D, Winter M, Thiede S, Herrmann C (2015) Energy efficient process chain: the impact of cutting fluid strategies. Procedia CIRP 29:360–365. https://doi.org/10.1016/2Fj.procir.2015.02.056

28. Pervaiz S, Anwar S, Qureshi I, Ahmed N (2019) Recent advances in the machining of titanium alloys using minimum quantity lubrication (MQL) based techniques. Int J Precis Eng Manuf-Green Technol 6:133–145. https://doi.org/10.1007/s40684-019-00033-4

29. Sadeghi MH, Hadad MJ, Tawakoli T, Vesali A, Emami M (2010) An investigation on surface grinding of AISI 4140 hardened steel using minimum quantity lubrication-MQL technique. IntJ Mater Form 3(4):241–251. https://doi.org/10.1007/s12289-009-0678-3

30. Sharma VS, Singh G, Sørby K (2015) A review on minimum quantity lubrication for machining processes. Mater Manuf Processes 30(8):935–953. https://doi.org/10.1080/10426914.2014.994759

31. Srikant RR, Rao PN (2017) Use of vegetable-based cutting fluids for sustainable machining. In J. P. Davim (Ed.). Sustainable machining. Materials forming, machining and tribology. Springer. https://doi.org/10.1007/978-3-319-51961-6_2

32. Moraes DL, Garcia MV, Lopes JC, Ribeiro FSF, Sanchez LEA, Foschini CR, Mello HJ, Aguiar PR, Bianchi EC (2019) Performance of SAE 52100 steel grinding using MQL technique with pure and diluted oil. Int J Adv Manuf Technol 105:4211–4223. https://doi.org/10.1007/s00170-019-04582-5

33. Said Z, Gupta M, Hegab H, Arora N, Khan AM, Jamil M, Bellos E (2019) A comprehensive review on minimum quantity lubrication (MQL) in machining process using nano-cutting fluids. Int J Adv Manuf Technol 105:2057–2086. https://doi.org/10.1007/s00170-019-04382-x

34. Lopes JC, Garcia MV, Volpato RS, Mello HJ, Ribeiro FSF, Sanchez LEA, Rocha KO, Neto LD, Aguiar PR, Bianchi EC (2020) Application of MQL technique using TiO₂ nanoparticles compared to MQL simultaneous to the grinding wheel cleaning jet. Int J Adv Manuf Technol 106:2205–2218. https://doi.org/10.1007/s00170-019-04760-5

35. Sawicki J, Kruszyński B, Wójcik R (2017) The influence of grinding conditions on the distribution of residual stress in the surface layer of 17CrNi6–6 steel after carburizing. Adv Sci Technol Res J 11(2):17–22. https://doi.org/10.12913/22998624/67671

36. Stachurski W, Krupanek K, Januszewicz B, Rosik R, Wójcik R (2018) An effect of grinding on microhardness and residual stress in 20MnCr5 following single-piece flow low-pressure carburizing. J Mach Eng 18(4):73–85. https://doi.org/10.5604/01.3001.0012.7634

37. Stachurski W, Sawicki J, Januszewicz B, Rosik R (2022) The influence of the depth of grinding on the condition of the surface layer of 20MnCr5 steel ground with the minimum quantity lubrication (MQL) method. Materials 15:1336. https://doi.org/10.3390/ma15041336

38. Wu W, Li C, Yang M, Zhang Y, Jia D, Hou Y, Li R, Cao H, Han Z (2019) Specific energy and G ratio of grinding cemented carbide under different cooling and lubrication conditions. Int J Adv Manuf Technol 105:67–82. https://doi.org/10.1007/s00170-019-04156-5

39. Morgan MN, Barczak L, Batako A (2012) Temperatures in fine grinding with minimum quantity lubrication (MQL). Int J Adv Manuf Technol 60:951–958. https://doi.org/10.1007/s00170-011-3678-7

40. Stachurski W, Sawicki J, Krupanek K, Nadolny K (2021) Application of numerical simulation to determine ability of air used in MQL method to clean grinding wheel active surface during sharpening of hob cutters. Int J Precis Eng Manuf-Green Technol 8:1095–1112. https://doi.org/10.1007/s40684-020-00239-x

41. Bianchi EC, Sato BK, Sales AR, Lopes JC, de Mello HJ, de Angelo Sanchez LE, Diniz AE, Aguiar PR (2018) Evaluating the effect of the compressed air wheel cleaning in grinding the AISI 4340 steel with CBN and MQL with water. Int J Adv Manuf Technol 95:2855–2864. https://doi.org/10.1007/s00170-017-1433-4

42. Javaroni RL, Lopes JC, Garcia MV, Ribeiro FSF, de Angelo Sanchez LE, de Mello HJ, Aguiar PR, Bianchi EC (2020) Grinding hardened steel using MQL associated with cleaning system and CBN wheel. Int J Adv Manuf Technol 107:2065–2080. https://doi.org/10.1007/s00170-020-05169-1

43. Lopes JC, Fragoso KM, Garcia MV, Ribeiro FSF, Francelin AP, de Angelo Sanchez LE, Rodrigues AR, de Mello HJ, Aguiar PR, Bianchi EC (2019) Behavior of hardened steel grinding using MQL under cold air and MQL CBN wheel cleaning. Int J Adv Manuf Technol 105:4373–4387. https://doi.org/10.1007/s00170-019-04571-8

44. Lee P-H, Lee SW (2011) Experimental characterization of micro-grinding process using compressed chilly air. Int J Mach Tools Manuf 51:201–209. https://doi.org/10.1016/j.ijmachtools.2010.11.010

45. Choi HZ, Lee SW, Jeong HD (2001) A comparison of the cooling effects of compressed cold air and coolant for cylindrical grinding with a CBN wheel. J Mater Process Technol 111(1–3):265–268. https://doi.org/10.1016/S0924-0136(01)00531-3

46. Lopes JC, Garcia MV, Valentim M, Javaroni RL, Ribeiro FSF, de Angelo Sanchez LE, de Mello HJ, Aguiar PR, Bianchi EC (2019) Grinding performance using variants of the MQL technique: MQL with cooled air and MQL simultaneous to the wheel cleaning jet. Int J Adv Manuf Technol 105:4429–4442. https://doi.org/10.1007/s00170-019-04574-5

47. Lopes JC, de Martini Fernandes L, Garcia MV, Moretti GB, de Moraes DL, Ribeiro FSF, de Angelo Sanchez LE, de Oliveira RFM, de Mello HJ, Aguiar PR, Bianchi EC (2020) Performance of austempered ductile iron (ADI) grinding using diluted oil in MQL combined with wheel cleaning jet and different CBN grains friability. Int J Adv Manuf Technol 107:1805–1818. https://doi.org/10.1007/s00170-020-05142-y

48. Ramesh K, Yeo SH, Zhong ZW, Huang H (2003) Ecological grinding with chilled air as coolant. Proc Inst Mech Eng Part B J Eng Manuf 217(3):409–419. https://doi.org/10.1243/2F095440503321590569

49. Stachurski W, Sawicki J, Wójcik R, Nadolny K (2018) Influence of application of hybrid MQL-CCA method of applying coolant during hob cutter sharpening on cutting blade surface condition. J Clean Prod 171:892–910. https://doi.org/10.1016/j.jclepro.2017.10.059

50. Stachurski W, Nadolny K (2018) Influence of the condition of the surface layer of a hob cutter sharpened using the MQL-CCA hybrid method of coolant provision on its operational wear. Int J Adv Manuf Technol 98:2185–2200. https://doi.org/10.1007/s00170-018-2379-x

51. Stachurski W, Wójcik R (2015) Method for introducing cooling agent to the grinding area during sharpening of blades of the hobbing cutter. Patent Number: PAT.222435

52. Tawakoli T, Hadad M, Sadeghi MH, Daneshi A, Sadeghi B (2011) Minimum quantity lubrication in grinding: effects of abrasive and coolant-lubricant types. J Clean Prod 19(17–18):2088–2099. https://doi.org/10.1016/2Fj.jclepro.2011.06.020

53. Choi HZ, Lee SW, Jeong HD (2002) The cooling effects of compressed cold air in cylindrical grinding with alumina and CBN wheels. J Mater Process Technol 127:155–158. https://doi.org/10.1016/S0924-0136(02)00117-6

54. Nguyen T, Zhang LC (2003) An assessment of the applicability of cold air and oil mist in surface grinding. J Mater Process Technol 140:224–230. https://doi.org/10.1016/S0924-0136(03)00714-3

55. Stachurski W, Sawicki J, Krupanek K, Nadolny K (2019) Numerical analysis of coolant flow in the grinding zone. Int J Adv Manuf Technol 104:1999–2012. https://doi.org/10.1007/s00170-019-03966-x

56. Alberdi R, Sanchez JA, Pombo I, Ortega N, Izquierdo B, Plaza S, Barrenetxea D (2011) Strategies for optimal use fluids in grinding. Int J Mach Tools Manuf 51:491–499. https://doi.org/10.1016/j.ijmachtools.2011.02.007

57. Baumgart C, Radziwill JJ, Kuster F, Wegener K (2017) A study of the interaction between coolant jet nozzle flow and the air-flow around a grinding wheel in cylindrical grinding. Procedia CIRP 58:517–522. https://doi.org/10.1016/j.procir.2017.03.261

58. Li C, Zhang X, Zhang Q, Wang S, Zhang D, Jia D, Zhang Y (2014) Modeling and simulation of useful fluid flow rate in grinding. Int J Adv Manuf Technol 75:1587–1604. https://doi.org/10.1007/s00170-014-6257-x

59. Mihić SD, Cioc S, Marinescu ID, Weismiller MC (2013) Detailed study of a fluid flow and heat transfer in the abrasive grinding contact using computational fluid dynamics methods. J Manuf Sci Eng 135(4):1–13. https://doi.org/10.1115/1.4023719

60. Mihić S, Dražumerič R, Pušavec F, Badger J, Krajnik P (2017) The use of computational fluid dynamics in the analysis of fluid flow and thermal aspects in grinding. Proc Inst Mech Eng Part B J Eng Manuf 231(12):2103–2111. https://doi.org/10.1177/2F0954405415624657

61. Vesali A, Tawakoli T (2014) Study on hydrodynamic pressure in grinding contact zone considering grinding parameters and grinding wheel specifications. Procedia CIRP 14:13–18. https://doi.org/10.1016/j.procir.2014.03.053

62. Zhang J-Z, Tan X-M, Liu B, Zhu X-D (2013) Investigation for convective heat transfer on grinding work-piece surface subjected to an impinging jet. Appl Therm Eng 51:653–661. https://doi.org/10.4028/www.scientific.net/AMM.249-250.434

63. Adibi H, Rezaei SM, Sarhan AAD (2014) Investigation on using high-pressure fluid jet in grinding process for less wheel loaded areas. Int J Adv Manuf Technol 70:2233–2240. https://doi.org/10.1007/s00170-013-5471-2

64. Gopan V, Wins LD (2016) Quantitative analysis of grinding wheel loading using image processing. Procedia Technol 25:885–891. https://doi.org/10.1016/j.protcy.2016.08.198

65. Catalogue (2020) NORTON.SAINT-GOBAIN 2021 Rozwiązania przemysłowe. Retrieved 3 Dec 2021, from https://www.nortonabrasives.com/sga-common/files/document/katnortonprzemyslowy_2021.pdf

66. WNT (2021) Cool-jet 6910.15.3–7. Retrieved 22 Nov 2021, from https://cuttingtools.ceratizit.com/pl/pl/products/81900100.html

67. Acharya S, Kanani Y (2017) Chapter three – advances in film cooling heat transfer. Adv Heat Transf 49:91–156. https://doi.org/10.1016/bs.aiht.2017.10.001

68. Burdet A, Abhari RS, Rose MG (2006) Modeling of film cooling—part II: model for use in three-dimensional computational fluid dynamics. J Turbomach 129(2):221–231. https://doi.org/10.1115/1.2437219

69. Fu W, Chao W, Tsubokura M, Li C, Wang W (2018) Direct numerical simulation of film cooling with a fan-shaped hole under low Reynolds number conditions. Int J Heat Mass Transf 123:544–560. https://doi.org/10.1016/j.ijheatmasstransfer.2018.03.011

70. Jiang Y, Murray A, di Mare L, Ireland P (2022) Mesh sensitivity of RANS simulations on film cooling flow. Int J Heat Mass Transf 182:121825. https://doi.org/10.1016/j.ijheatmasstransfer.2021.121825

71. Sparrow EM, Gorman JM, Abraham JP, Minkowycz W (2017) Chapter one – validation of turbulence models for numerical simulation of fluid flow and convective heat transfer. Adv Heat Transf 49:1–35. https://doi.org/10.1016/bs.aiht.2017.09.002

72. Menter FR (1994) Two-equation eddy-viscosity turbulence models for engineering applications. AIAA J 32(8):1598–1605. https://doi.org/10.2514/3.12149

73. Kato M, Launder BE (1993) The modeling of turbulent flow around stationary and vibrating square cylinders. In Proceedings of the 9th Symposium on Turbulent Shear Flows. Kyoto, Japan, 10.4.1–10.4.6

74. Katritsis D, Kaiktsis L, Chaniotis A, Pantos J, Efstathopoulos EP, Marmarelis V (2007) Wall shear stress: theoretical considerations and methods of measurement. Prog Cardiovasc Dis 49(5):307–329. https://doi.org/10.1016/j.pcad.2006.11.001

75. Liu X, Li Z, Gao N (2018) An improved wall shear stress measurement technique using sandwiched hot-film sensors. Theor Appl Mech Lett 8(2):137–141. https://doi.org/10.1016/j.taml.2018.02.010

76. Bianco G (2004) Gear hobbing. Novaprint, Bologna

77. Hall H (2007) Tool and cutter sharpening. Special Interest Model Books Ltd, Hemel Hempstead

78. Molyduval (2020) EC-Safety Data Sheet, Biocut 3000. Retrieved 3 Dec 2021 from www.molyduval.com

79. Orlen Oil (2021) Emulgol ES-12. Retrieved 3 Dec 2021 from www.orlenoil.pl/oodownload/pds/en/27435

80. Delta Optical (2021) Mikroskop cyfrowy Delta Optical Smart 2MP PRO. Retrieved 3 Dec 2021 from http://deltaoptical.pl/mikroskop-cyfrowy-delta-optical-smart-5mp-pro?pdf=1

81. Michalska J, Chmiela B (2014) Phase analysis in duplex stainless steel: comparison of EBSD and quantitative metallography methods. IOP Conf Ser Mater Sci Eng 55:012010. https://doi.org/10.1088/1757-899X/55/1/012010

Publisher's note Springer Nature remains neutral with regard to jurisdictional claims in published maps and institutional affiliations.